Chinese Journal of Polymer Science Vol. 31, No. 9, (2013), 1250–1259

Chinese Journal of Polymer Science
© Chinese Chemical Society
Institute of Chemistry, CAS
Springer-Verlag Berlin Heidelberg 2013

DEVIATIONS FROM BULK MORPHOLOGIES IN THIN FILMS OF BLOCK COPOLYMER/ADDITIVE BINARY BLENDS*

Xin-yu Wei[a], Wei-yin Gu[a], Xiao-bo Shen[a], Joseph Strzalka[b], Zhang Jiang[b] and Thomas P. Russell[a**]

[a] *Department of Polymer Science and Engineering, University of Massachusetts, Amherst, Massachusetts 01003, USA*
[b] *X-ray Science Division, Argonne National Laboratory, Argonne, Illinois 60439, USA*

Abstract Deviations from bulk morphologies in thin films of binary blends of alkyne-functionalized diblock copolymer poly(ethylene oxide)-*block*-poly(*n*-butyl methacrylate-*random*-propargyl methacrylate) (PEO-*b*-P(*n*BMA-*r*-PgMA)) and Rhodamine B azide are reported, where thermal click reaction between the two components leads to microphase separated morphologies. Both in the bulk and in thin films, increasing the azide loading ratio resulted in the transition from a lamellar microdomain morphology to a hexagonally packed cylindrical mircodomain morphology. However, in thin films the lamellae-cylinder transition was observed at a different azide loading ratio, which was determined by film thickness. As a result, significant deviations from the bulk morphology were observed. These results indicate that surface interactions and confined geometry can play an important role in dictating the morphology in thin films of BCP/additive binary blends.

Keywords: Block copolymer; Morphology; Thin film.

INTRODUCTION

Block copolymers (BCPs), consisting of two or more chemically different chain segments that are connected at one end *via* covalent bonding, microphase separate into a series of ordered array within 10–100 nm, such as lamellar, hexagonally packed cylindrical and body-centered cubic spherical microdomains and a gyroid bicontinuous structure[1]. Thin films of BCPs have been demonstrated as promising templates and scaffolds for the fabrication of nanostructured materials[2–7], which can then be used for a variety of applications, such as semiconductor devices[8, 9], magnetic storage media[10, 11] and filtration membranes[12]. While the phase behavior of bulk BCPs is determined by Flory-Huggins parameter (χ), total degree of polymerization (N) and volume fraction of each block (f)[13, 14], in BCP thin films, boundary conditions, such as interfacial interactions and confined geometry due to film thickness, also strongly dictate the morphology. Therefore, additional issues need to be considered in thin films. For example, due to the interactions between the blocks and the substrate and/or the free surface, the microdomains will assume an orientation in the thin films. In the case of preferential interactions, the microdomains are oriented parallel to the substrate[15–17].

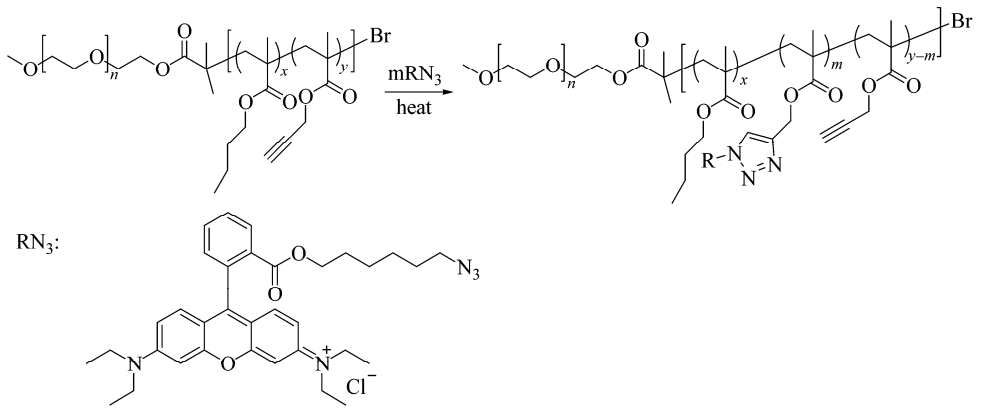
Due to the effects of interfacial interactions and confined geometries arising from film thickness, the

* This work was financially supported by the Department of Energy Office of Basic Energy Science under Contract No. DE-FG02-96ER45612(XW, TPR design of experiments, synthesis of BCP) and the NSF-supported Materials Research Science and Engineering Center and the NSF-supported Center for Hierarchical Manufacturing at University of Massachusetts Amherst(XS, WG, assistance with the GISAXS measurements). Use of the Advanced Photon Source, an Office of Science User Facility operated for the U.S. Department of Energy Office of Science by Argonne National Laboratory, was supported by the U.S. DOE under Contract No. DE-AC02-06CH11357. Use of the Advanced Light Source is supported by the Director, Office of Science, Office of Basic Energy Sciences, of the U.S. Department of Energy under Contract No. DE-AC02-05CH11231.
** Corresponding author: Thomas P. Russell, E-mail: russell@mail.pse.umass.edu
Invited paper dedicated to the memory of Prof. Bingzheng Jiang
Received March 25, 2013; Revised April 23, 2013; Accepted April 26, 2013
doi: 10.1007/s10118-013-1320-x

morphology in thin films can also deviate from that of bulk samples. For instance, both theoretical[18, 19] and experimental[20–24] studies have confirmed that, in thin films of asymmetric BCPs, if the substrate preferentially interacts with one block, the microphase separated structures can differ from those in the bulk samples. For BCPs with bulk morphological transitions, the transition temperatures in thin films can shift from bulk values, and the transition pathway may also be different. For example, order-to-disorder transitions (ODTs) in thin films of polystyrene-*block*-poly(methyl methacrylate) (PS-*b*-PMMA)[25, 26] and polystyrene-*block*-polyisoprene (PS-*b*-PI)[27] di-BCPs were investigated on a variety of substrates. When the substrate has strong preferential interactions with one block, composition fluctuations are enhanced. As a result, the ODT transition temperature T_{ODT} in thin films is higher than the bulk value and increases as the film thickness decreases[25, 27]. When the preferential interaction is weak, the surface effects on the T_{ODT} in thin films also become less significant[27]. On the other hand, for BCP thin films on substrates with balanced interactions, T_{ODT} decreases as the film becomes thinner[26]. Thin films of BCPs with bulk order-to-order transitions (OOTs) were also studied[28–32]. The transition temperatures were found to shift from the corresponding bulk values. In addition, some microphase separated morphologies that were observed in the bulk may not appear in thin films[28, 30, 31].

Recently, incorporating additives has been suggested as a convenient approach to tailor the morphology of BCPs. Especially, if the additive selectively associates with one block of a BCP *via* specific interactions, for example metal ion coordination[33–36] and hydrogen bonding[37–40], both the chemical structure and composition of the BCP may be changed, which results in a series of morphological transition, such as disorder-to-order transitions (DOTs)[40–42] and OOTs[37, 41, 43, 44]. These selective-associating additives also have substantial effects on the morphology of BCPs in thin film geometries. For example, salt complexes were shown to have significant effects on the orientation and lateral ordering of BCP microdomains in thin films during solvent annealing[45, 46].

Previously we reported the use of Rhodamine B azide as a novel additive to induce DOTs of an alkyne-functionalized BCP poly(ethylene oxide)-*block*-poly(*n*-butyl methacrylate-*random*-propargyl methacrylate) (PEO-*b*-P(*n*BMA-*r*-PgMA))[47–50]. While the neat BCP is in phase mixed state, when it is blended with the azide and annealed at elevated temperatures, the azide is attached to the polymer backbone *via* thermal alkyne/azide click chemistry (Scheme 1). As a result, non-favorable interactions between the two blocks are significantly increased, and well-defined microphase separated morphologies can be thus obtained. Especially, we have demonstrated that the DOTs induced by click reaction can be also realized in thin film geometries, and the orientation of microdomains in thin films is affected by the loading ratio of azide additive and film thickness[50].



Scheme 1 Alkyne/azide click reaction between the PEO-*b*-P(*n*BMA-*r*-PgMA) di-BCP and Rhodamine B azide

In this paper, we continued to investigate the DOTs induced by click reaction in thin films and focused on a special case of such BCP/additive binary blend thin films, where the microphase separated morphology after click reaction was not only determined by the azide loading ratio, but also affected by film thickness. Therefore, significant deviations from bulk morphologies were observed. These results indicate that surface interactions and

confined geometry can play important roles in dictating the thin film morphologies of BCP/additive binary blends.

EXPERIMENTAL

Materials

PEO-*b*-P(*n*BMA-*r*-PgMA) di-BCPs and Rhodamine B azide were synthesized as described previously[47]. 1,1,2-Trichloroethane (96%) was purchased from Sigma-Aldrich and used as received. Si (100) wafers with *ca*. 2 nm native oxide layer were purchased from International Wafer Service and cleaned with oxygen plasma for 5−10 min before use.

Instruments

Recently, grazing incidence small angle X-ray scattering (GISAXS) was widely used to explore the nanoscaled structures in thin films of BCPs[51–53]. GISAXS experiments were performed at the beamline 8-ID-E, Advanced Photon Source (APS), Argonne National Laboratory (ANL), Argonne, IL[54]. The wavelength of incident X-ray was 0.1688 nm, the sample-to-detector distance was 1641.0 mm, and scattering signals were collected by a marCCD 2D detector with a resolution of 79 μm/pixel. The measurements were performed with the sample in the open air with typical exposure time 30–90 s.

Scanning force microscopy (SFM) characterizations were performed using a Multiple-mode Nanoscope III SFM instrument (Digital Instruments) in the tapping mode with commercial Si cantilevers. Film thickness was measured by ellipsometry.

Sample Preparation

The PEO-*b*-P(*n*BMA-*r*-PgMA) di-BCP and Rhodamine B azide were weighed separately according to a pre-determined azide loading ratio, which is defined as the mole ratio between the azide and alkyne groups, *i.e.*, the mole ratio between Rhodamine B azide and the PgMA repeating unites. The typical azide loading ratio ranged from 50% to 130%, and previously we have shown that, both in bulk and in thin films, if the azide is in moderate excess, after the thermal click reaction, well-defined microphase separated structures can still be obtained[49, 50]. The two components were then dissolved together in 1,1,2-trichloroethane, a good solvent for both components. The solution was spin-coated on Si (100) wafers and the thin films were annealed at elevated temperatures under vacuum.

RESULTS AND DISCUSSION

The PEO-*b*-P(*n*BMA-*r*-PgMA) BCP investigated here, denoted as 10.5-11-40 in our previous report[47], has a molecular weight of 10.5 kg/mol for the PEO block and 11 kg/mol for the P(*n*BMA-*r*-PgMA) block. On average, each polymer chain has 40 PgMA repeating units, corresponding to roughly a 1:1 mole ratio between the *n*BMA and PgMA comonomers. As reported previously, while other di-BCPs showed the same type of morphology with the azide loading ratio ranging from 50% (mole ratio, related to the alkyne groups in the BCP) to 115%, 10.5-11-40 showed a lamellar microdomain morphology at 50% azide loading ratio but hexagonally packed cylindrical microdomain morphologies at the azide loading ratio of 75% or above[49]. Such lamellae-cylinder transition can be explained by the change in the volume fraction of each block due to the change of azide loading ratio. Previously several researchers have shown that, for binary blends of BCP and selectively-interacting additives, as the loading ratio of additive varies, different microphase separated morphologies can be obtained[42, 44, 55]. In our case, we have estimated that, for the binary blend of 10.5-11-40 and Rhodamine B azide, as the azide loading ratio increases from 50% to 115%, after click reaction, the volume fraction of PEO block decreases from 31% to 21%, which may correspond to the phase boundary between lamellar microdomain morphology and hexagonally packed cylindrical morphology[49]. In addition, the change in azide loading ratio may also change the value of χ between the PEO block and the modified P(*n*BMA-*r*-PgMA) block, which may also contribute to the morphology transition, as has been confirmed in binary blends of PS-*b*-PMMA BCP and lithium ion[41].

We first investigated thin films of the BCP/additive binary blend with the film thickness of *ca*. 80 nm. As

can be seen from Fig. 1(c), at the azide loading ratio of 100%, after annealing at 110 °C for 12 h, worm-like textures on the top surface were observed from the SFM height image. The corresponding GISAXS pattern (Fig. 1f) shows Bragg rod scattering peaks extending along q_z, indicating in-plane structures. These results indicate the presence of a lamellar microdomains morphology aligned normal to the substrate. The lamellar microdomains with a perpendicular orientation is further confirmed by the very weak second order reflections at the position of $q/q^* = 2/1$, as can be seen from both the GISAXS pattern and the corresponding one-dimensional integration (Fig. 2). These results clearly reveal a deviation from the bulk morphology, where a hexagonally packed cylindrical microdomain morphology was observed.

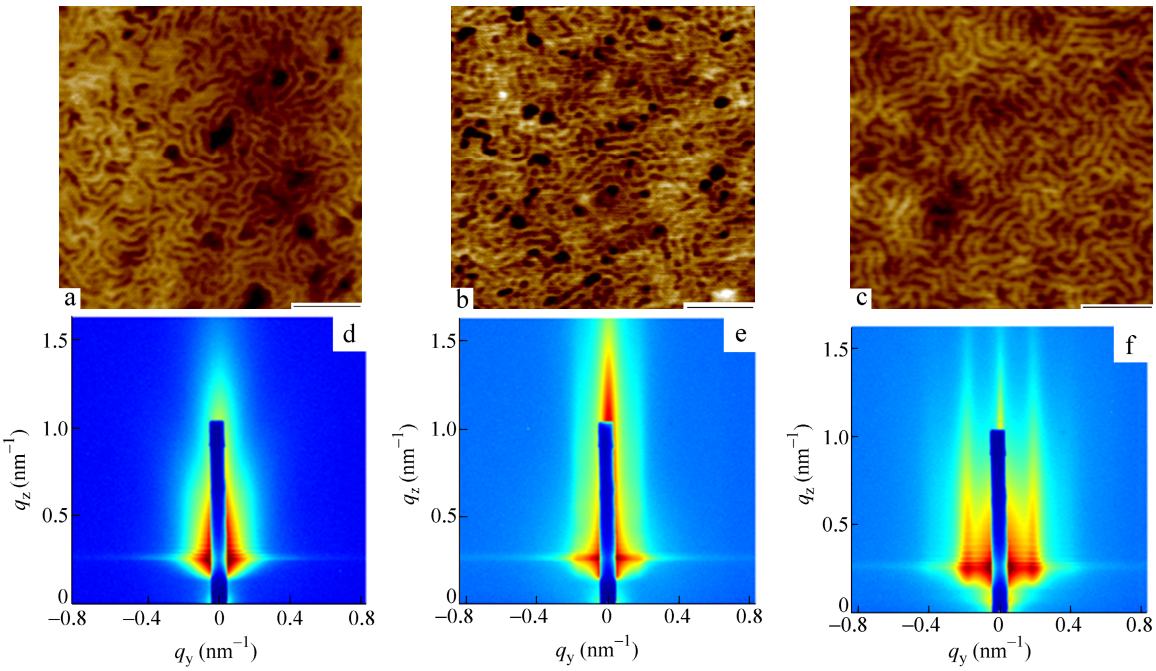


Fig. 1 SFM height images (a–c) and GISAXS patterns (d–f) of thin films of binary blends of PEO-*b*-P(*n*BMA-*r*-PgMA) di-BCP 10.5-11-40 and Rhodamine B azide, at the azide loading ratio of 50% (a, d), 75% (b, e) and 100% (c, f)
All the samples were annealed at 110 °C for 12 h. Film thickness is around 80 nm. Scale bar is 200 nm. GISAXS incident angle is 0.20°.

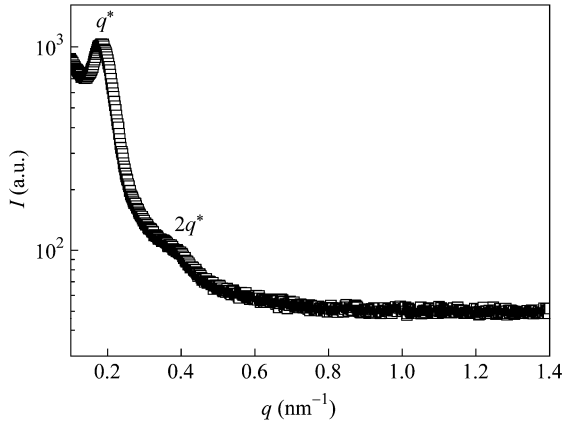


Fig. 2 GISAXS q_y line profiles at q_z = 0.5 nm^{-1} of the thin film of binary blend of PEO-*b*-P(*n*BMA-*r*-PgMA)di-BCP 10.5-11-40 and Rhodamine B azide, at the azide loading ratio of 100%
The sample was annealed at 110 °C for 12 h. Film thickness is around 80 nm.

We then kept the film thickness around 80 nm and changed the azide loading ratio. The azide loading ratio was first decreased to 75% and 50%. Since previously it has been confirmed that both in bulk and in thin films, if the azide loading ratio is around or below 25%, microphase separated structure could not be obtained[49, 50], we didn't further decrease the azide loading ratio. As can be seen from Figs. 1(a), 1(b), 1(d) and 1(e), at both azide loading ratios, worm-like textures on the top surface were observed from the SFM height images, and Bragg rod scattering peaks were seen in the corresponding GISAXS patterns, indicating lamellar microdomain morphologies with a perpendicular orientation. However, in the bulk a lamellar microdomain morphology was only observed at 50% azide loading ratio, so it is clear that the thin film morphologies at 75% azide ratio is still different from the corresponding bulk morphologies.

On the other hand, when the azide loading ratio was increased above 100%, we could clearly see the change in thin film morphology. At the azide loading ratio of 115%, as can be seen from the SFM height image (Fig. 3a), worm-like textures were dominant on the top surface, but some circular structures could be also seen. The corresponding GISAXS pattern (Fig. 3c) showed Bragg rod scattering peaks extending along q_z. These results suggest that while the majority of the BCP microphase separates to form lamellar microdomains with a perpendicular orientation, a small amount of cylindrical microdomains is also present. As the azide loading ratio was further increased to 130%, circular structure was observed from the SFM height image (Fig. 3b), and Bragg rod scattering peaks along q_z were observed in the corresponding GISAXS pattern (Fig. 3d), indicating hexagonally packed cylindrical microdomains oriented normal to the substrate. These observations reveal that, similar to the bulk samples, in thin films, as the azide loading ratio increases, the morphology after the click-reaction-induced DOT also evolves from a lamellar microdomain morphology to a hexagonally packed cylindrical microdomain morphology. However, in thin films, this transition occurs at a much higher azide loading ratio. As a result, significant deviations from bulk morphologies were observed over a wide range of alkyne/azide ratio.

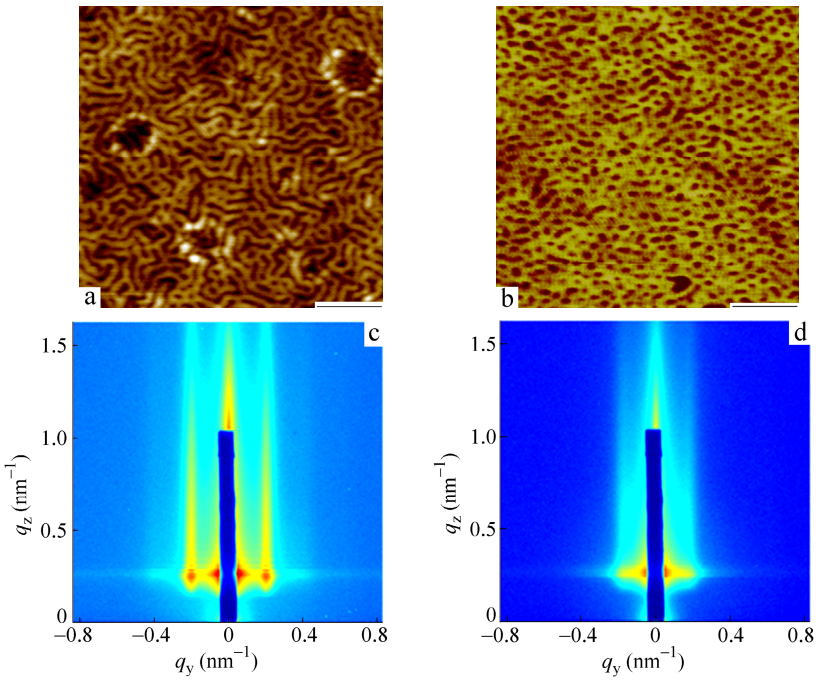


Fig. 3 SFM height images (a, b) and GISAXS patterns (c, d) of thin films of binary blend of PEO-*b*-P(*n*BMA-*r*-PgMA) di-BCP 10.5-11-40 and Rhodamine B azide, at the azide loading ratio of 115% (a, c) and 130% (b, d)
All the samples were annealed at 110 °C for 12 h. Film thickness is around 80 nm. Scale bar is 200 nm. GISAXS incident angle is 0.20°.

We then investigated thin films of the binary blend with different thickness. The film thickness was first decreased to *ca*. 40 nm. From the SFM height images and GISAXS patterns we can see that, at the azide loading ratio of 100%, after annealing at 110 °C for 12 h, the SFM height image showed circular structures on the top surface, and sharp Bragg rod scattering peaks extending along q_z were seen in the corresponding GISAXS pattern, which indicates a hexagonally packed cylindrical microdomain morphology with a perpendicular orientation of the microdomains, the same as the corresponding bulk morphology (Figs. 4c and 4f). Similarly, at the azide loading ratio of 115% and 130%, cylindrical microdomains with a perpendicular orientation were also observed (Figs. 5a, 5b, 5c and 5e). However, when the azide loading ratio was decreased to 75%, although some circular structures could still be observed from the SFM height image, most of the top surface was covered with worm-like textures (Fig. 4b). When the azide loading ratio was further decreased to 50%, after annealing, the top surface only showed worm-like structures (Fig. 4a). For both azide loading ratios, the corresponding GISAXS patterns (Figs. 4d and 4e) showed Bragg rod scattering peaks extending along q_z, indicating in-plane structure. Since the film thickness is now close to one natural period, the results may correspond to either a lamellar microdomain morphology with a perpendicular orientation or a hexagonally packed cylindrical microdomain morphology with a parallel orientation. However, according to our previous report, at the film thickness of *ca*. 40 nm, the microdomains should still have a strong tendency to orient perpendicular to the substrate at 50% azide loading ratio[50]. Therefore, the microphase separated structures at 50% and 75% azide loading ratios should correspond to lamellar microdomains with a perpendicular orientation. It is thus evident that, as the film thickness decreased to *ca*. 40 nm, the transition between lamellar and cylindrical morphologies occurs in the range of 75%–100% azide loading ratio. However, this phase boundary is still different from the corresponding bulk one, so morphology deviation was still observed at 75% azide loading ratio.

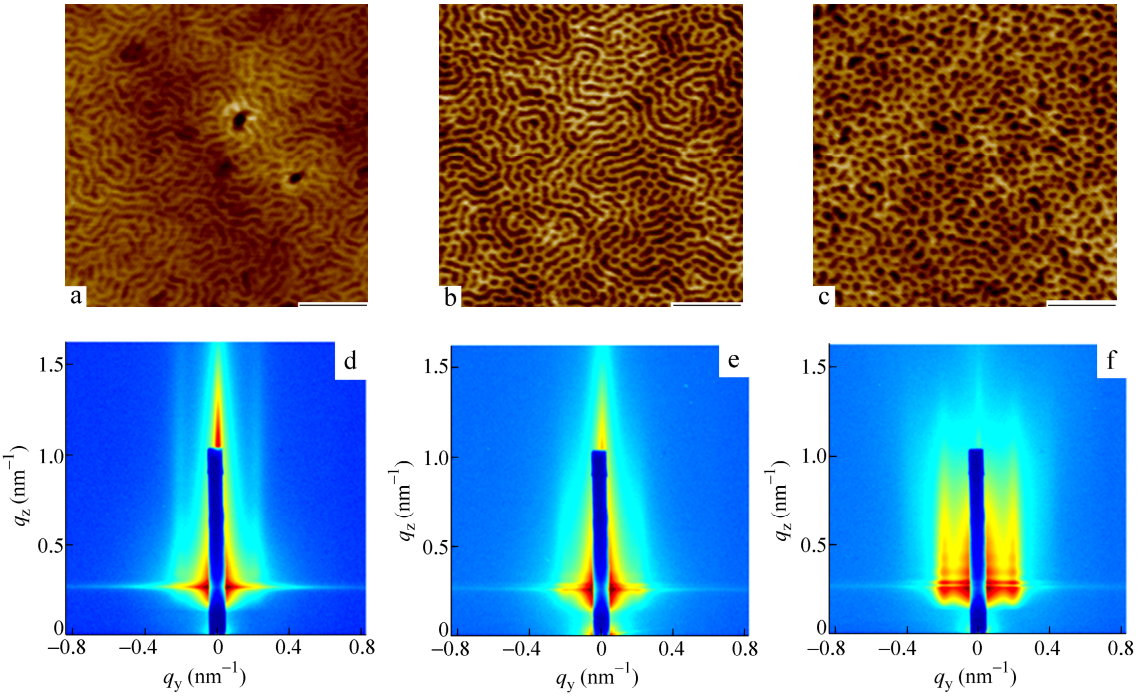


Fig. 4 SFM height images (a–c) and GISAXS patterns (d–f) of thin films of binary blend of PEO-*b*-P(*n*BMA-*r*-PgMA) di-BCP 10.5-11-40 and Rhodamine B azide, at the azide loading ratio of 50% (a, d), 75% (b, e) and 100% (c, f)
All the samples were annealed at 110 °C for 12 h. Film thickness is around 40 nm. Scale bar is 200 nm. GISAXS incident angle is 0.20°.

The film thickness was further decreased to *ca*. 25 nm. As can be seen from the SFM images and GISAXS patterns shown in Fig. 6, at all three azide loading ratios, the GISAXS patterns showed Bragg-rod scattering peaks along q_z. At the azide loading ratio of 75% and 100%, circular structures were observed on the top surface,

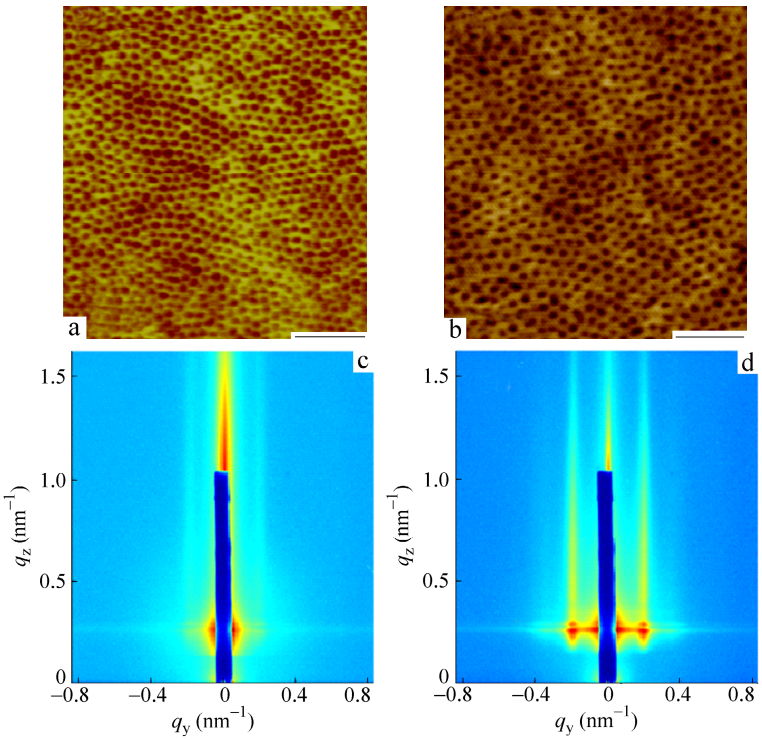


Fig. 5 SFM height images (a, b) and GISAXS patterns (c, d) of thin films of binary blend of PEO-*b*-P(*n*BMA-*r*-PgMA) di-BCP 10.5-11-40 and Rhodamine B azide, at the azide loading ratio of 115% (a, c) and 130% (b, d) All the samples were annealed at 110 °C for 12 h. Film thickness is around 40 nm. Scale bar is 200 nm. GISAXS incident angle is 0.20°.

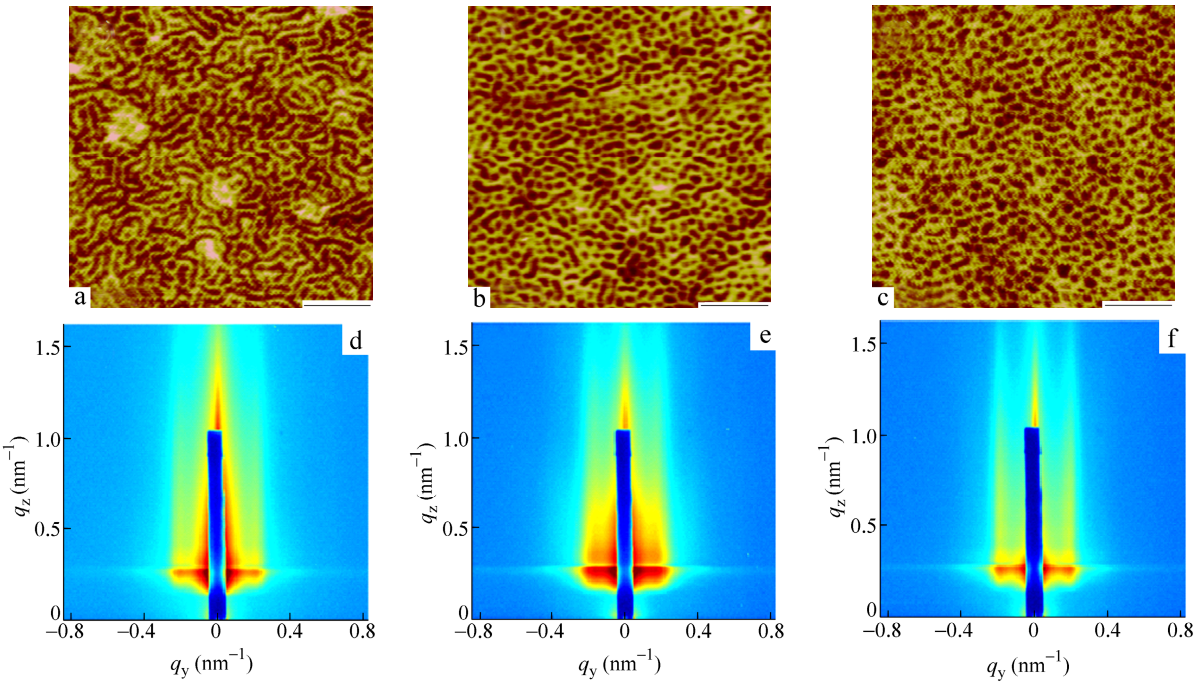


Fig. 6 SFM height images (a–c) and GISAXS patterns (d–f) of thin films of binary blend of PEO-*b*-P(*n*BMA-*r*-PgMA) di-BCP 10.5-11-40 and Rhodamine B azide, at the azide loading ratio of 50% (a, d), 75% (b, e) and 100% (c, f), respectively All the samples were annealed at 110 °C for 12 h. Film thickness is around 25 nm. Scale bar is 200 nm. GISAXS incident angle is 0.20°.

indicating hexagonally packed cylindrical microdomain morphologies with a perpendicular orientation. Similarly, at the azide loading ratio of 115% and 130%, cylindrical microdomains aligned normal to the substrate were also observed (data not shown). On the other hand, as the azide loading ratio was decreased to 50%, worm-like textures were observed instead, which corresponds to a lamellar microdomain morphology with a perpendicular orientation. These results clearly suggest that a hexagonally packed cylindrical microdomain morphology with a perpendicular orientation was observed when the azide loading ratio was 75% or above. The lamellae-cylinder transition now occurred at the same range of azide loading ratio as bulk samples, so no deviation from the bulk morphology was observed.

Figure 7 shows the SFM height images and GISAXS patterns of thin films of the binary blend with the thickness around 150 nm. We can see that, at the azide loading ratio of 130%, while cylindrical microdomains were observed with the film thickness of 80 nm or below, as the film becomes thicker, most of the top surface showed worm-like textures, although in some areas circular structures were observed. The corresponding GISAXS pattern still showed Bragg rod scattering peaks along q_z. These results clearly suggest that, as film thickness increases, lamellar microdomains are dominant in the thin film. At the azide loading ratio of 115%, after thermal annealing, a lamellar structure with the microdomains normal to the substrate was also observed, similar to the sample with the film thickness of *ca*. 80 nm. It is thus evident that, as film thickness increases, the lamellae-cylinder boundary further shifts to higher azide loading ratios, resulting in deviations from bulk morphologies over a wider range of alkyne/azide ratio.

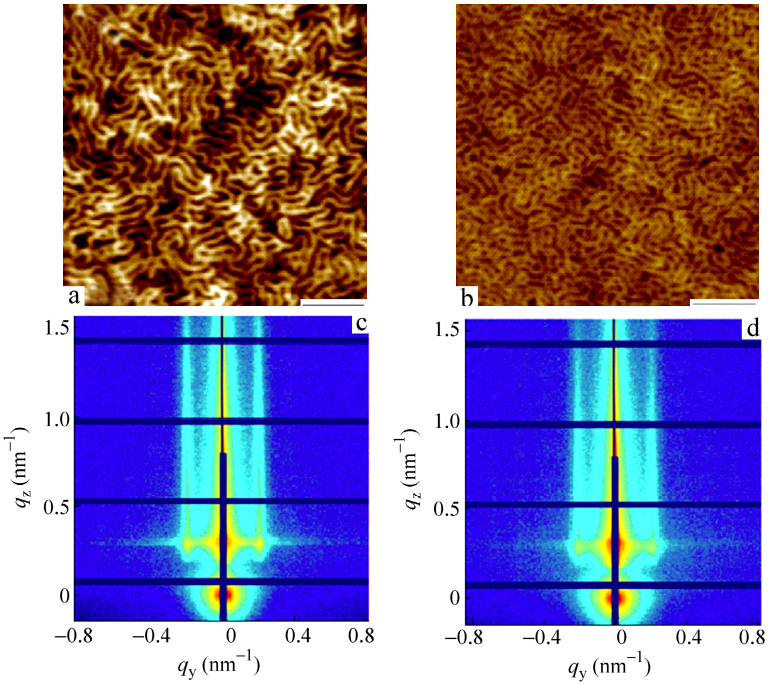


Fig. 7 SFM height images (a, b) and GISAXS patterns (c, d) of thin films of binary blend of PEO-*b*-P(*n*BMA-*r*-PgMA) BCP 10.5-11-40 and Rhodamine B azide with the azide loading ratio of 115% (a, c) and 130% (b, d) Film thickness is around 150 nm. All the samples were annealed at 110 °C for 12 h. Scale bar is 200 nm. GISAXS incident angle is 0.20°.

Figure 8 further summarizes the morphology of thin films of binary blend of di-BCP 10.5-11-40 and Rhodamine B azide at different azide loading ratios and film thickness. As can be seen, at all the azide loading ratios and film thickness, the microdomains have a strong tendency to orient perpendicular to the substrate, similar to our previous investigation[50]. However, the thin film morphology of binary blend of 10.5-11-40 and Rhodamine B azide is more significantly affected by film thickness. While both in the bulk and in thin films, increasing the azide loading ratio leads to a transition from the lamellar morphology to the hexagonally packed cylindrical morphology, in thin films, the range of azide loading ratio that corresponds to the transition is strongly dependent on the film thickness. As the film thickness increases, this phase boundary shifts to higher

azide loading ratios. As a result, deviation from bulk morphology is more significant in thicker films. One possible explanation is that, since after click reaction, the BCP 10.5-11-40 is located at the boundary between the regimes of lamellar and cylindrical phases, the effects of surface interaction and confinement may be sufficient enough to cause the thin film morphologies to differ from the corresponding bulk ones.

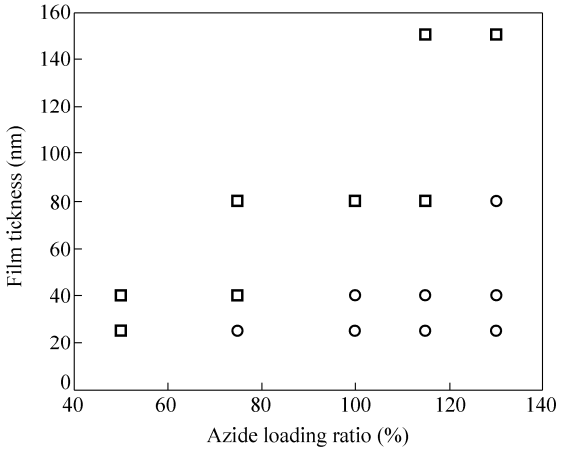


Fig. 8 Summary of of binary blend of PEO-*b*-P(*n*BMA-*r*-PgMA) BCP 10.5-11-40 and Rhodamine B azide Open squares indicate that in the film a lamellar microdomain morphology with a perpendicular orientation is dominant. Open circles indicate that in the thin film a hexagonally packed cylindrical microdomain morphology with a perpendicular orientation is dominant.

Due to the increased film roughness in thicker films, further increasing the film thickness was not successful, and thus we are not clear if film thickness will continue to affect the lamellae-cylinder transition. A possible situation is, as the film thickness further increases, since the effects of interfacial interactions and confined geometry become weaker[56], the microphase separated morphology in the center of the film may be the same as the one in the bulk. However, in the regime close to the top and bottom surface, deviation from bulk morphologies may still exist.

CONCLUSIONS

In summary, we have demonstrated that the thin film morphologies of binary blends of BCP 10.5-11-40 and Rhodamine B azide are highly dependent on film thickness, showing significant deviations from the bulk samples. This is very different from our previous investigations, where film thickness only affected the orientation of microdomains[50]. Strikingly, while the effects of surface interactions and confined geometry usually become weaker as film thickness increases, in our cases, the deviation becomes more significant in thicker films. Our results indicate that, similar to thin films of neat BCPs, in thin films of BCP/additive binary blends, surface interactions and confined geometry can also play an important role in dictating the morphology and result in deviation from bulk samples.

REFERENCES

1 Bates, F.S. and Fredrickson, G.H., Phys. Today, 1999, 52: 32
2 Fasolka, M.J. and Mayes, A.M., Annu. Rev. Mater. Res., 2001, 31: 323
3 Hawker, C.J. and Russell, T.P., MRS Bull., 2005; 30: 952
4 Segalman, R.A., Mater. Sci. Eng. Rep., 2005, R48: 191
5 Li, M. and Ober, C.K., Mater. Today, 2006, 9: 30
6 Park, C., Yoon, J. and Thomas, E.L., Polymer, 2003, 44: 6725
7 Bang, J., Jeong, U., Ryu, D.Y., Russell, T.P. and Hawker, C.J., Adv. Mater., 2009, 21: 4769
8 Black, C.T., Guarini, K.W., Milkove, K.R., Baker, S.M., Russell, T.P. and Tuominen, M.T., Appl. Phys. Lett., 2001, 79: 409
9 Black, C.T., Ruiz, R., Breyta, G., Cheng, J.Y., Colburn, M.E., Guarini, K.W., Kim, H.C. and Zhang, Y., IBM J. Res. Dev., 2007, 51: 605

10 Cheng, J.Y., Ross, C.A., Chan, V.Z.H., Thomas, E.L., Lammertink, R.G.H. and Vancso, G.J., Adv. Mater., 2001, 13: 1174
11 Ross, C.A., Haratani, S., Castano, F.J., Hao, Y., Hwang, M., Shima, M., Cheng, J.Y., Vogeli, B., Farhoud, M., Walsh, M. and Smith, H.I., J. Appl. Phys., 2002, 91: 6848
12 Yang, S.Y., Ryu, I., Kim, H.Y., Kim, J.K., Jang, S.K. and Russell, T.P., Adv. Mater., 2006, 18: 709
13 Bates, F.S. and Fredrickson, G.H., Annu. Rev. Phys. Chem., 1990, 41: 525
14 Fredrickson, G.H. and Bates, F.S., Annu. Rev. Mater. Sci., 1996, 26: 501
15 Anastasiadis, S.H., Russell, T.P., Satija, S.K. and Majkrzak, C.F., Phys. Rev. Lett., 1989, 62: 1852
16 Russell, T.P., Coulon, G., Deline, V.R. and Miller, D.C., Macromolecules, 1989, 22: 4600
17 Huang, E., Mansky, P., Russell, T.P., Harrison, C., Chaikin, P.M., Register, R.A., Hawker, C.J. and Mays, J., Macromolecules, 2000, 33: 80
18 Turner, M.S., Rubinstein, M. and Marques, C.M., Macromolecules, 1994, 27: 4986
19 Tan, H., Yan, D. and Shi, A.C., Macromolecules, 2004, 37: 9646
20 Knoll, A., Horvat, A., Lyakhova, K.S., Krausch, G., Sevink, G.J.A., Zvelindovsky, A.V. and Magerle, R., Phys. Rev. Lett., 2002, 89: 035501
21 Liu, Y., Zhao, W., Zheng, X., King, A., Singh, A., Rafailovich, M.H., Sokolov, J., Dai, K.H., Kramer, E.J., Schwarz, S.A., Gebizlioglu, O. and Sinha, S.K., Macromolecules, 1994, 27: 4000
22 Karim, A., Singh, N., Sikka, M., Bates, F.S., Dozier, W.D. and Felcher, G.P., J. Chem. Phys., 1994, 100: 1620
23 Park, I., Park, S., Park, H.W., Chang, T., Yang, H.C. and Ryu, C.Y., Macromolecules, 2006, 39: 315
24 Tsarkova, L., Knoll, A., Krausch, G. and Magerle, R., Macromolecules, 2006, 39: 3608
25 Kim, E., Ahn, H., Ryu, D.Y., Kim, J. and Cho, J., Macromolecules, 2009, 42: 8385
26 Kim, E., Choi, S., Guo, R., Ryu, D.Y., Hawker, C.J. and Russell, T. R., Polymer, 2010, 51: 6313
27 Shin, C., Ahn, H., Kim, E., Ryu, D. Y., Huh, J., Kim, K. W., and Russell, T. P., Macromolecules, 2008, 41: 9140
28 Shin, C., Ryu, D.Y., Huh, J., Kim, J.H. and Kim, K.W., Macromolecules, 2009, 42: 2157
29 Sohn, K.E., Kojio, K., Berry, B.C., Karim, A., Coffin, R.C., Bazan, G.C., Kramer, E.J., Sprung, M. and Wang, J., Macromolecules, 2010, 43: 3406
30 Ahn, H., Shin, C., Lee, B. and Ryu, D.Y., Macromolecules, 2010, 43: 1958
31 Jung, J., Park, H.W., Lee, S., Lee, H., Chang, T., Matsunaga, K. and Jinnai, H., ACS Nano, 2010, 4: 3109
32 Arceo, A. and Green, P.F., J. Phys. Chem. B, 2005, 109: 6958
33 Ruzette, A.V.G., Soo, P.P., Sadoway, D.R. and Mayes, A.M., J. Electrochemical Soc., 2001, 148: A53
34 Epps, T.H., Bailey, T.S., Pham, H.D. and Bates, F.S., Chem. Mater., 2002, 14: 1706
35 Lee, D.H., Kim, H.Y, Kim, J.K., Huh, J. and Ryu, D.Y., Macromolecules, 2006, 39: 2027
36 Wang, J.Y., Xu T., Leiston-Belanger, J.M., Gupta, S. and Russell, T.P., Phys. Rev. Lett., 2006, 96: 128301
37 Zhao, J.Q., Pearce, E.M. and Kwei, T.K., Macromolecules, 1997, 30: 7119
38 Ruokolainen, J., Saariaho, M., Ikkala, O., ten Brinke, G., Thomas, E.L., Torkkeli, M. and Serimaa R., Macromolecules, 1999, 32: 1152
39 Sidorenko, A., Tokarev, I., Minko, S. and Stamm, M., J. Am. Chem. Soc., 2003, 125: 12211
40 Tirumala, V.R., Romang, A., Agarwal, S., Lin, E.K. and Watkins, J.J., Adv. Mater., 2008, 20: 1603
41 Wang, J.Y., Chen, W., Roy, C., Sievert, J.D. and Russell, T.P., Macromolecules, 2008, 41: 963
42 Miranda, D.F., Russell, T.P. and Watkins, J.J., Macromolecules, 2010, 43: 10528
43 Dobrosielska, K., Wakao, S., Takano, A. and Matsushita, Y., Macromolecules, 2008, 41: 7695
44 Chen, S.C., Kuo, S.W., Jeng, U.S., Su, C.J. and Chang, F.C., Macromolecules, 2010, 43: 1083
45 He, J., Wang, J.Y., Xu, J., Tangirala, R., Shin, D., Russell, T.P., Li, X. and Wang, J., Adv. Mater., 2007, 19: 4370
46 Kim, S.H., Misner, M.J., Yang, L., Gang, O., Ocko, B.M. and Russell, T.P., Macromolecules, 2006, 39: 8473
47 Wei, X., Chen, W., Chen, X. and Russell, T.P., Macromolecules, 2010, 43: 6234
48 Wei, X., Li, L., Kalish, J.P., Chen, W. and Russell, T.P., Macromolecules, 2011, 44: 4269
49 Wei, X., Strzalka, J.W., Li, L. and Russell, T.P., J. Polym. Sci. Part B: Polym. Phys., 2012, 50: 55
50 Wei, X., Gu, W., Chen, W., Shen, X., Liu, F., Strzalka, J.W., Jiang, Z. and Russell, T.P., Soft Matter, 2012, 8: 5273
51 Renaud, G., Lazzari, R. and Leroy, F., Sur. Sci. Rep., 2009, 64: 255
52 Lee, B., Park, I., Yoon, J., Park, S., Kim, J., Kim, K.W., Chang, T. and Ree, M., Macromolecules, 2005, 38: 4311
53 Busch, P., Posselt, D., Smilgies, D.M., Rauscher, M. and Papadakis, C.M., Macromolecules, 2007, 40: 630
54 Jiang, Z., Li, X., Strzalka, J., Sprung, M., Sun, T., Sandy, A.R., Narayanan, S., Lee, D.R. and Wang, J., J. Synchr. Rad., 2012, 19: 6234
55 Tirumala, V.R., Daga, V., Bosse, A.W., Romang, A., Ilavsky, J., Lin, E.K. and Watkins, J.J., Macromolecules, 2008, 41: 7978
56 Xu, T., Hawker, C.J. and Russell, T.P., Macromolecules, 2005, 38: 2802